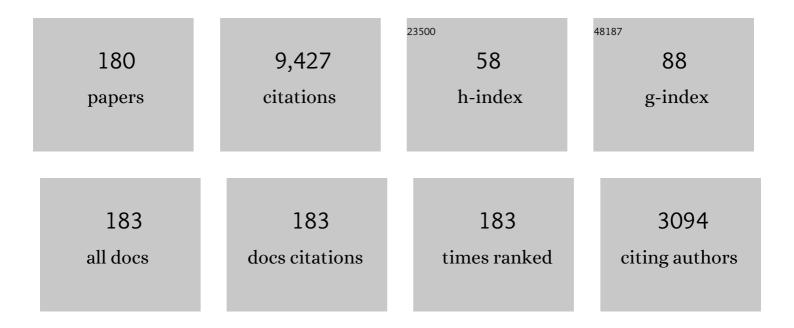
Marko Knezevic

List of Publications by Year in descending order

Source: https://exaly.com/author-pdf/406726/publications.pdf Version: 2024-02-01



#	Article	IF	CITATIONS
1	Deformation twinning in AZ31: Influence on strain hardening and texture evolution. Acta Materialia, 2010, 58, 6230-6242.	3.8	558
2	Strain rate and temperature effects on the selection of primary and secondary slip and twinning systems in HCP Zr. Acta Materialia, 2015, 88, 55-73.	3.8	216
3	Strain rate and temperature sensitive multi-level crystal plasticity model for large plastic deformation behavior: Application to AZ31 magnesium alloy. International Journal of Plasticity, 2016, 83, 90-109.	4.1	177
4	Three dimensional predictions of grain scale plasticity and grain boundaries using crystal plasticity finite element models. Computer Methods in Applied Mechanics and Engineering, 2014, 277, 239-259.	3.4	155
5	Modeling bending of α-titanium with embedded polycrystal plasticity in implicit finite elements. Materials Science & Engineering A: Structural Materials: Properties, Microstructure and Processing, 2013, 564, 116-126.	2.6	153
6	Integration of self-consistent polycrystal plasticity with dislocation density based hardening laws within an implicit finite element framework: Application to low-symmetry metals. Journal of the Mechanics and Physics of Solids, 2013, 61, 2034-2046.	2.3	146
7	A dislocation density based crystal plasticity finite element model: Application to a two-phase polycrystalline HCP/BCC composites. Journal of the Mechanics and Physics of Solids, 2014, 66, 16-31.	2.3	145
8	A strain-rate and temperature dependent constitutive model for BCC metals incorporating non-Schmid effects: Application to tantalum–tungsten alloys. International Journal of Plasticity, 2014, 62, 93-104.	4.1	143
9	A polycrystal plasticity model for predicting mechanical response and texture evolution during strain-path changes: Application to beryllium. International Journal of Plasticity, 2013, 49, 185-198.	4.1	141
10	Deformation twinning in rolled WE43-T5 rare earth magnesium alloy: Influence on strain hardening and texture evolution. Acta Materialia, 2017, 131, 221-232.	3.8	138
11	A study of microstructure-driven strain localizations in two-phase polycrystalline HCP/BCC composites using a multi-scale model. International Journal of Plasticity, 2015, 74, 35-57.	4.1	137
12	Explicit incorporation of deformation twins into crystal plasticity finite element models. Computer Methods in Applied Mechanics and Engineering, 2015, 295, 396-413.	3.4	133
13	A dislocation density based elasto-plastic self-consistent model for the prediction of cyclic deformation: Application to AA6022-T4. International Journal of Plasticity, 2015, 72, 200-217.	4.1	133
14	Low cycle fatigue behavior of direct metal laser sintered Inconel alloy 718. International Journal of Fatigue, 2016, 93, 156-167.	2.8	132
15	Crystal plasticity simulations using discrete Fourier transforms. Acta Materialia, 2009, 57, 1777-1784.	3.8	131
16	Microstructure and mechanical behavior of direct metal laser sintered Inconel alloy 718. Materials Characterization, 2016, 113, 1-9.	1.9	130
17	A crystal plasticity model incorporating the effects of precipitates in superalloys: Application to tensile, compressive, and cyclic deformation of Inconel 718. International Journal of Plasticity, 2017, 99, 162-185.	4.1	127
18	In situ X-ray diffraction and crystal plasticity modeling of the deformation behavior of extruded Mg–Li–(Al) alloys: An uncommon tension–compression asymmetry. Acta Materialia, 2015, 86, 254-268.	3.8	123

#	Article	lF	CITATIONS
19	Modeling mechanical response and texture evolution of α-uranium as a function of strain rate and temperature using polycrystal plasticity. International Journal of Plasticity, 2013, 43, 70-84.	4.1	118
20	Computationally efficient database and spectral interpolation for fully plastic Taylor-type crystal plasticity calculations of face-centered cubic polycrystals. International Journal of Plasticity, 2008, 24, 1264-1276.	4.1	115
21	Dual-phase steel sheets under cyclic tension–compression to large strains: Experiments and crystal plasticity modeling. Journal of the Mechanics and Physics of Solids, 2016, 96, 65-87.	2.3	115
22	Texture evolution in two-phase Zr/Nb lamellar composites during accumulative roll bonding. International Journal of Plasticity, 2014, 57, 16-28.	4.1	112
23	Experimental characterization and crystal plasticity modeling of anisotropy, tension-compression asymmetry, and texture evolution of additively manufactured Inconel 718†at room and elevated temperatures. International Journal of Plasticity, 2020, 125, 63-79.	4.1	111
24	Anisotropic stress–strain response and microstructure evolution of textured α-uranium. Acta Materialia, 2012, 60, 702-715.	3.8	109
25	An elasto-plastic self-consistent model with hardening based on dislocation density, twinning and de-twinning: Application to strain path changes in HCP metals. Materials Science & Engineering A: Structural Materials: Properties, Microstructure and Processing, 2015, 638, 262-274.	2.6	104
26	Fast computation of first-order elastic–plastic closures for polycrystalline cubic-orthorhombic microstructures. Computational Materials Science, 2007, 39, 643-648.	1.4	102
27	Grain size and orientation distributions: Application to yielding of α-titanium. Acta Materialia, 2009, 57, 2339-2348.	3.8	96
28	Effect of dislocation density-twin interactions on twin growth in AZ31 as revealed by explicit crystal plasticity finite element modeling. International Journal of Plasticity, 2017, 99, 81-101.	4.1	96
29	Spectral calibration of crystal plasticity models. Acta Materialia, 2006, 54, 1795-1804.	3.8	95
30	Anomalous Basal Slip Activity in Zirconium under High-strain Deformation. Materials Research Letters, 2013, 1, 133-140.	4.1	93
31	Role of grain structure, grain boundaries, crystallographic texture, precipitates, and porosity on fatigue behavior of Inconel 718 at room and elevated temperatures. Materials Characterization, 2019, 149, 184-197.	1.9	93
32	Coupling elasto-plastic self-consistent crystal plasticity and implicit finite elements: Applications to compression, cyclic tension-compression, and bending to large strains. International Journal of Plasticity, 2017, 93, 187-211.	4.1	92
33	Mechanical response, twinning, and texture evolution of WE43 magnesium-rare earth alloy as a function of strain rate: Experiments and multi-level crystal plasticity modeling. International Journal of Plasticity, 2019, 120, 180-204.	4.1	88
34	Deformation behavior of the cobalt-based superalloy Haynes 25: Experimental characterization and crystal plasticity modeling. Acta Materialia, 2014, 63, 162-168.	3.8	86
35	Elastic–plastic property closures for hexagonal close-packed polycrystalline metals using first-order bounding theories. Acta Materialia, 2007, 55, 2729-2737.	3.8	81
36	A high-performance computational framework for fast crystal plasticity simulations. Computational Materials Science, 2014, 83, 101-106.	1.4	81

#	Article	IF	CITATIONS
37	Application of microstructure sensitive design to structural components produced from hexagonal polycrystalline metals. Computational Materials Science, 2008, 43, 374-383.	1.4	80
38	Building texture evolution networks for deformation processing of polycrystalline fcc metals using spectral approaches: Applications to process design for targeted performance. International Journal of Plasticity, 2010, 26, 1183-1194.	4.1	79
39	Bulk texture evolution of nanolamellar Zr–Nb composites processed via accumulative roll bonding. Acta Materialia, 2015, 92, 97-108.	3.8	79
40	Delineation of first-order closures for plastic properties requiring explicit consideration of strain hardening and crystallographic texture evolution. International Journal of Plasticity, 2008, 24, 327-342.	4.1	78
41	Effect of age hardening on the deformation behavior of an Mg–Y–Nd alloy: In-situ X-ray diffraction and crystal plasticity modeling. Materials Science & Engineering A: Structural Materials: Properties, Microstructure and Processing, 2015, 628, 396-409.	2.6	76
42	Compressive, shear, and fracture behavior of CNT reinforced Al matrix composites manufactured by severe plastic deformation. Materials and Design, 2016, 106, 112-119.	3.3	75
43	Anisotropic modeling of structural components using embedded crystal plasticity constructive laws within finite elements. International Journal of Mechanical Sciences, 2016, 105, 227-238.	3.6	74
44	Determining volume fractions of γ, γ′, γ″, Î′, and MC-carbide phases in Inconel 718 as a function of its processing history using an advanced neutron diffraction procedure. Materials Science & Engineering A: Structural Materials: Properties, Microstructure and Processing, 2020, 781, 139228.	2.6	74
45	A new implementation of the spectral crystal plasticity framework in implicit finite elements. Mechanics of Materials, 2015, 84, 114-126.	1.7	72
46	Latent hardening within the elasto-plastic self-consistent polycrystal homogenization to enable the prediction of anisotropy of AA6022-T4 sheets. International Journal of Plasticity, 2018, 105, 141-163.	4.1	68
47	Texture evolution and enhanced grain refinement under high-pressure-double-torsion. Materials Science & Engineering A: Structural Materials: Properties, Microstructure and Processing, 2014, 611, 29-36.	2.6	67
48	Procedures for reducing large datasets of crystal orientations using generalized spherical harmonics. Mechanics of Materials, 2015, 88, 73-86.	1.7	67
49	A numerical procedure enabling accurate descriptions of strain rate-sensitive flow of polycrystals within crystal visco-plasticity theory. Computer Methods in Applied Mechanics and Engineering, 2016, 308, 468-482.	3.4	67
50	Material-based design of the extrusion of bimetallic tubes. Computational Materials Science, 2014, 95, 63-73.	1.4	66
51	Texture formation in orthorhombic alpha-uranium under simple compression and rolling to high strains. Journal of Nuclear Materials, 2016, 473, 143-156.	1.3	66
52	Deep drawing simulations using the finite element method embedding a multi-level crystal plasticity constitutive law: Experimental verification and sensitivity analysis. Computer Methods in Applied Mechanics and Engineering, 2019, 354, 245-270.	3.4	65
53	Explicit modeling of double twinning in AZ31 using crystal plasticity finite elements for predicting the mechanical fields for twin variant selection and fracture analyses. Acta Materialia, 2018, 157, 339-354.	3.8	64
54	Spectral database solutions to elasto-viscoplasticity within finite elements: Application to a cobalt-based FCC superalloy. International Journal of Plasticity, 2015, 70, 151-165.	4.1	62

#	Article	IF	CITATIONS
55	Activity of pyramidal I and II <c+a> slip in Mg alloys as revealed by texture development. Journal of the Mechanics and Physics of Solids, 2018, 111, 290-307.</c+a>	2.3	61
56	The plasticity of highly oriented nano-layered Zr/Nb composites. Acta Materialia, 2016, 115, 189-203.	3.8	60
57	Average intragranular misorientation trends in polycrystalline materials predicted by a viscoplastic self-consistent approach. Acta Materialia, 2016, 104, 228-236.	3.8	60
58	Deformation and fracture mechanisms in WE43 magnesium-rare earth alloy fabricated by direct-chill casting and rolling. Materials Science & Engineering A: Structural Materials: Properties, Microstructure and Processing, 2018, 726, 194-207.	2.6	60
59	Representation of the orientation distribution function and computation of first-order elastic properties closures using discrete Fourier transforms. Acta Materialia, 2009, 57, 3916-3923.	3.8	59
60	High-Pressure Double Torsion as a Severe Plastic Deformation Process: Experimental Procedure and Finite Element Modeling. Journal of Materials Engineering and Performance, 2015, 24, 1471-1482.	1.2	59
61	An implicit formulation of the elasto-plastic self-consistent polycrystal plasticity model and its implementation in implicit finite elements. Mechanics of Materials, 2019, 136, 103065.	1.7	59
62	Microstructure and mechanical properties of carbon nanotubes reinforced aluminum matrix composites synthesized via equal-channel angular pressing. Materials Science & Engineering A: Structural Materials: Properties, Microstructure and Processing, 2016, 670, 205-216.	2.6	58
63	Modelling recrystallization textures driven by intragranular fluctuations implemented in the viscoplastic self-consistent formulation. Acta Materialia, 2019, 164, 530-546.	3.8	57
64	A crystallographic extension to the Olson-Cohen model for predicting strain path dependence of martensitic transformation. Acta Materialia, 2019, 166, 386-401.	3.8	56
65	Effects of build orientation and heat treatment on the evolution of microstructure and mechanical properties of alloy Mar-M-509 fabricated via laser powder bed fusion. International Journal of Plasticity, 2019, 121, 116-133.	4.1	54
66	A new visco-plastic self-consistent formulation implicit in dislocation-based hardening within implicit finite elements: Application to high strain rate and impact deformation of tantalum. Computer Methods in Applied Mechanics and Engineering, 2018, 341, 888-916.	3.4	53
67	Modeling discrete twin lamellae in a microstructural framework. Scripta Materialia, 2016, 121, 84-88.	2.6	52
68	Enhancement of orientation gradients during simple shear deformation by application of simple compression. Journal of Applied Physics, 2015, 117, .	1.1	51
69	Enhanced microstructural homogeneity in metal-matrix composites developed under high-pressure-double-torsion. Materials Characterization, 2015, 104, 92-100.	1.9	50
70	Microstructure and texture evolution in Mg/Nb layered materials made by accumulative roll bonding. International Journal of Plasticity, 2020, 125, 1-26.	4.1	50
71	Modeling of the thermo-mechanical response and texture evolution of WE43 Mg alloy in the dynamic recrystallization regime using a viscoplastic self-consistent formulation. International Journal of Plasticity, 2020, 130, 102705.	4.1	50
72	Modeling of Sheet Metal Forming Based on Implicit Embedding of the Elasto-Plastic Self-Consistent Formulation in Shell Elements: Application to Cup Drawing of AA6022-T4. Jom, 2017, 69, 922-929.	0.9	48

Marko Knezevic

#	Article	IF	CITATIONS
73	Transitioning rate sensitivities across multiple length scales: Microstructure-property relationships in the Taylor cylinder impact test on zirconium. International Journal of Plasticity, 2016, 84, 138-159.	4.1	47
74	Modeling of intragranular misorientation and grain fragmentation in polycrystalline materials using the viscoplastic self-consistent formulation. International Journal of Plasticity, 2018, 109, 193-211.	4.1	46
75	Residual Ductility and Microstructural Evolution in Continuous-Bending-under-Tension of AA-6022-T4. Materials, 2016, 9, 130.	1.3	45
76	Origin of texture development in orthorhombic uranium. Materials Science & Engineering A: Structural Materials: Properties, Microstructure and Processing, 2016, 665, 108-124.	2.6	44
77	Multiscale Modeling of Microstructureâ€Property Relationships of Polycrystalline Metals during Thermoâ€Mechanical Deformation. Advanced Engineering Materials, 2018, 20, 1700956.	1.6	44
78	Predicting intragranular misorientation distributions in polycrystalline metals using the viscoplastic self-consistent formulation. Acta Materialia, 2017, 140, 398-410.	3.8	43
79	Rate and temperature dependent deformation behavior of as-cast WE43 magnesium-rare earth alloy manufactured by direct-chill casting. Materials Science & Engineering A: Structural Materials: Properties, Microstructure and Processing, 2018, 712, 50-64.	2.6	43
80	Room temperature deformation mechanisms of Mg/Nb nanolayered composites. Journal of Materials Research, 2018, 33, 1311-1332.	1.2	43
81	Effect of hot working and aging heat treatments on monotonic, cyclic, and fatigue behavior of WE43 magnesium alloy. Materials Science & Engineering A: Structural Materials: Properties, Microstructure and Processing, 2019, 747, 27-41.	2.6	43
82	Computer implementations of iterative and non-iterative crystal plasticity solvers on high performance graphics hardware. Computational Mechanics, 2015, 56, 677-690.	2.2	41
83	Compact reconstruction of orientation distributions using generalized spherical harmonics to advance large-scale crystal plasticity modeling: Verification using cubic, hexagonal, and orthorhombic polycrystals. Acta Materialia, 2018, 155, 418-432.	3.8	41
84	Predicting elastic anisotropy of dual-phase steels based on crystal mechanics and microstructure. International Journal of Mechanical Sciences, 2019, 151, 639-649.	3.6	40
85	High-performance full-field crystal plasticity with dislocation-based hardening and slip system back-stress laws: Application to modeling deformation of dual-phase steels. Journal of the Mechanics and Physics of Solids, 2020, 134, 103750.	2.3	40
86	Stress-assisted (γ→αâ€2) and strain-induced (γ→ε→αâ€2) phase transformation kinetics laws implemented i plasticity model for predicting strain path sensitive deformation of austenitic steels. International Journal of Plasticity, 2021, 136, 102807.	n a crystal 4.1	40
87	Characterization of Crystallographic Texture and Intra-Grain Morphology in Cross-Rolled Tantalum. Metallurgical and Materials Transactions A: Physical Metallurgy and Materials Science, 2015, 46, 1085-1096.	1.1	39
88	Coupled texture and non-Schmid effects on yield surfaces of body-centered cubic polycrystals predicted by a crystal plasticity finite element approach. International Journal of Solids and Structures, 2017, 109, 22-32.	1.3	39
89	Elevated Temperature Effects on the Plastic Anisotropy of an Extruded Mg-4 Wt Pct Li Alloy: Experiments and Polycrystal Modeling. Metallurgical and Materials Transactions A: Physical Metallurgy and Materials Science, 2017, 48, 446-458.	1.1	39
90	OpenMP and MPI implementations of an elasto-viscoplastic fast Fourier transform-based micromechanical solver for fast crystal plasticity modeling. Advances in Engineering Software, 2018, 126, 46-60.	1.8	39

#	Article	IF	CITATIONS
91	Origins of high ductility exhibited by an extruded magnesium alloy Mg-1.8Zn-0.2Ca: Experiments and crystal plasticity modeling. Journal of Materials Science and Technology, 2021, 84, 27-42.	5.6	39
92	Over five-times improved elongation-to-fracture of dual-phase 1180 steel by continuous-bending-under-tension. Materials and Design, 2019, 161, 95-105.	3.3	38
93	Polycrystal plasticity modeling for load reversals in commercially pure titanium. International Journal of Plasticity, 2020, 125, 294-313.	4.1	37
94	Modelling the temperature and texture effects on the deformation mechanisms of magnesium alloy AZ31. International Journal of Mechanical Sciences, 2020, 182, 105727.	3.6	36
95	Three orders of magnitude improved efficiency with highâ€performance spectral crystal plasticity on GPU platforms. International Journal for Numerical Methods in Engineering, 2014, 97, 785-798.	1.5	35
96	Lowâ€cycle fatigue behavior of rolled WE43â€T5 magnesium alloy. Fatigue and Fracture of Engineering Materials and Structures, 2019, 42, 1357-1372.	1.7	35
97	A crystal plasticity finite element model embedding strain-rate sensitivities inherent to deformation mechanisms: Application to alloy AZ31. International Journal of Plasticity, 2021, 143, 103031.	4.1	35
98	Effect of microstructure induced anisotropy on fatigue behaviour of functionally graded Inconel 718 fabricated by additive manufacturing. Materials Characterization, 2021, 179, 111350.	1.9	35
99	An automated procedure for geometry creation and finite element mesh generation: Application to explicit grain structure models and machining distortion. Computational Materials Science, 2018, 141, 269-281.	1.4	34
100	A comparative study between elasto-plastic self-consistent crystal plasticity and anisotropic yield function with distortional hardening formulations for sheet metal forming. Mechanics of Materials, 2020, 148, 103422.	1.7	34
101	Predicting deformation behavior of α-uranium during tension, compression, load reversal, rolling, and sheet forming using elasto-plastic, multi-level crystal plasticity coupled with finite elements. Journal of the Mechanics and Physics of Solids, 2020, 138, 103924.	2.3	34
102	Predicting Texture Evolution in Ta and Ta-10W Alloys Using Polycrystal Plasticity. Jom, 2015, 67, 2670-2674.	0.9	33
103	Microstructure effects on the recrystallization of low-symmetry alpha-uranium. Journal of Nuclear Materials, 2015, 465, 189-195.	1.3	33
104	Identification of crystal plasticity model parameters by multi-objective optimization integrating microstructural evolution and mechanical data. Computer Methods in Applied Mechanics and Engineering, 2021, 379, 113747.	3.4	31
105	Spectral database constitutive representation within a spectral micromechanical solver for computationally efficient polycrystal plasticity modelling. Computational Mechanics, 2018, 61, 89-104.	2.2	31
106	Delineation of First-Order Elastic Property Closures for Hexagonal Metals Using Fast Fourier Transforms. Materials, 2015, 8, 6326-6345.	1.3	30
107	A multi-GPU implementation of a full-field crystal plasticity solver for efficient modeling of high-resolution microstructures. Computer Physics Communications, 2020, 254, 107231.	3.0	30
108	Origin of plastic anisotropy in (ultra)-fine-grained Mg–Zn–Zr alloy processed by isothermal multi-step forging and rolling: Experiments and modeling. Materials Science & Engineering A: Structural Materials: Properties, Microstructure and Processing, 2018, 713, 81-93.	2.6	29

#	Article	IF	CITATIONS
109	Review of microstructure and micromechanism-based constitutive modeling of polycrystals with a low-symmetry crystal structure. Journal of Materials Research, 2018, 33, 3711-3738.	1.2	29
110	Effects of heat treatment and build orientation on the evolution of ϵ and α′ martensite and strength during compressive loading of additively manufactured 304L stainless steel. Acta Materialia, 2020, 195, 59-70.	3.8	29
111	A numerical study into element type and mesh resolution for crystal plasticity finite element modeling of explicit grain structures. Computational Mechanics, 2021, 67, 33-55.	2.2	29
112	Modelling dynamic recrystallisation in magnesium alloy AZ31. International Journal of Plasticity, 2021, 142, 102995.	4.1	29
113	A generalized spherical harmonics-based procedure for the interpolation of partial datasets of orientation distributions to enable crystal mechanics-based simulations. Materialia, 2019, 6, 100328.	1.3	28
114	Non-acid, alcohol-based electropolishing enables high-quality electron backscatter diffraction characterization of titanium and its alloys: Application to pure Ti and Ti-6Al-4V. Materials Characterization, 2020, 166, 110406.	1.9	28
115	Modeling the role of local crystallographic correlations in microstructures of Ti-6Al-4V using a correlated structure visco-plastic self-consistent polycrystal plasticity formulation. Acta Materialia, 2021, 203, 116502.	3.8	28
116	A full-field crystal plasticity model including the effects of precipitates: Application to monotonic, load reversal, and low-cycle fatigue behavior of Inconel 718. Materials Science & Engineering A: Structural Materials: Properties, Microstructure and Processing, 2021, 803, 140478.	2.6	27
117	Experimental characterization and crystal plasticity modeling for predicting load reversals in AA6016-T4 and AA7021-T79. International Journal of Plasticity, 2022, 153, 103292.	4.1	27
118	Modeling of trans-grain twin transmission in AZ31 via a neighborhood-based viscoplastic self-consistent model. International Journal of Plasticity, 2019, 117, 21-32.	4.1	26
119	Experimental study of continuous-bending-under-tension of AA6022-T4. Journal of Materials Processing Technology, 2019, 266, 707-714.	3.1	24
120	Fabrication of a low alloy ultra-high strength (>1500†MPa yield) steel using powder bed fusion additive manufacturing. Materials Science & Engineering A: Structural Materials: Properties, Microstructure and Processing, 2020, 770, 138512.	2.6	23
121	Additive manufacturing of functionally graded inconel 718: Effect of heat treatment and building orientation on microstructure and fatigue behaviour. Journal of Materials Processing Technology, 2022, 306, 117573.	3.1	23
122	Crystal plasticity modeling of strain-induced martensitic transformations to predict strain rate and temperature sensitive behavior of 304ÂL steels: Applications to tension, compression, torsion, and impact. International Journal of Plasticity, 2022, 156, 103367.	4.1	23
123	Strengthening of alloy AA6022-T4 by continuous bending under tension. Materials Science & Engineering A: Structural Materials: Properties, Microstructure and Processing, 2019, 758, 47-55.	2.6	22
124	Modeling material behavior during continuous bending under tension for inferring the post-necking strain hardening response of ductile sheet metals: Application to DP 780 steel. International Journal of Mechanical Sciences, 2020, 174, 105508.	3.6	22
125	Characterization of microstructure in Nb rods processed by rolling: Effect of grooved rolling die geometry on texture uniformity. International Journal of Refractory Metals and Hard Materials, 2017, 66, 44-51.	1.7	20
126	Microstructure metrics for quantitative assessment of particle size and dispersion: Application to metal-matrix composites. Powder Technology, 2017, 311, 226-238.	2.1	20

#	Article	IF	CITATIONS
127	Thermo-hydrogen refinement of microstructure to improve mechanical properties of Ti–6Al–4V fabricated via laser powder bed fusion. Materials Science & Engineering A: Structural Materials: Properties, Microstructure and Processing, 2021, 809, 140980.	2.6	20
128	Mechanical behavior and texture evolution of WE43 magnesium-rare earth alloy in Split-Hopkinson Pressure Bar and Taylor Impact Cylinder Testing. International Journal of Impact Engineering, 2020, 143, 103589.	2.4	19
129	In-situ high-energy X-ray diffraction and crystal plasticity modeling to predict the evolution of texture, twinning, lattice strains and strength during loading and reloading of beryllium. International Journal of Plasticity, 2022, 150, 103217.	4.1	19
130	Experimental studies into the role of cyclic bending during stretching of dual-phase steel sheets. International Journal of Material Forming, 2020, 13, 393-408.	0.9	18
131	Elastic constants of pure body-centered cubic Mg in nanolaminates. Computational Materials Science, 2020, 174, 109501.	1.4	18
132	Effects of environmental temperature and sample pre-straining on high cycle fatigue strength of WE43-T5 magnesium alloy. International Journal of Fatigue, 2020, 141, 105903.	2.8	18
133	Plasticity and structure evolution of ferrite and martensite in DP 1180 during tension and cyclic bending under tension to large strains. Materials Science & Engineering A: Structural Materials: Properties, Microstructure and Processing, 2021, 820, 141536.	2.6	18
134	Experimental characterization and crystal plasticity modeling of dual-phase steels subjected to strain path reversals. Mechanics of Materials, 2022, 168, 104293.	1.7	18
135	Crystal Plasticity Modeling of Microstructure Evolution and Mechanical Fields During Processing of Metals Using Spectral Databases. Jom, 2017, 69, 830-838.	0.9	17
136	Inferring Post-Necking Strain Hardening Behavior of Sheets by a Combination of Continuous Bending Under Tension Testing and Finite Element Modeling. Experimental Mechanics, 2020, 60, 459-473.	1.1	17
137	Validation of recent analytical dilatational models for porous polycrystals using crystal plasticity finite element models with Schmid and non-Schmid activation laws. Mechanics of Materials, 2018, 126, 148-162.	1.7	16
138	Rare-earth- and aluminum-free, high strength dilute magnesium alloy for Biomedical Applications. Scientific Reports, 2020, 10, 15839.	1.6	16
139	Graphics processing unit accelerated phase field dislocation dynamics: Application to bi-metallic interfaces. Advances in Engineering Software, 2018, 115, 248-267.	1.8	15
140	Effects of Pressure and Number of Turns on Microstructural Homogeneity Developed in High-Pressure Double Torsion. Metallurgical and Materials Transactions A: Physical Metallurgy and Materials Science, 2017, 48, 1249-1263.	1.1	14
141	Modeling of plasticity-induced martensitic transformation to achieve hierarchical, heterogeneous, and tailored microstructures in stainless steels. CIRP Journal of Manufacturing Science and Technology, 2021, 33, 389-397.	2.3	14
142	Role of interface-affected dislocation motion on the strength of Mg/Nb nanolayered composites inferred by dual-mode confined layer slip crystal plasticity. Journal of the Mechanics and Physics of Solids, 2021, 152, 104421.	2.3	14
143	Application of Microstructure Sensitive Design to FCC Polycrystals. Materials Science Forum, 2007, 546-549, 675-680.	0.3	13
144	Strain-Rate Sensitivity, Tension-Compression Asymmetry, r-Ratio, Twinning, and Texture Evolution of a Rolled Magnesium Alloy Mg-1.3Zn-0.4Ca-0.4Mn. Metallurgical and Materials Transactions A: Physical Metallurgy and Materials Science, 2020, 51, 3858-3868.	1.1	13

#	Article	IF	CITATIONS
145	Effects of plasticity-induced martensitic transformation and grain refinement on the evolution of microstructure and mechanical properties of a metastable high entropy alloy. Journal of Alloys and Compounds, 2022, 891, 161871.	2.8	13
146	Coupling of a multi-GPU accelerated elasto-visco-plastic fast Fourier transform constitutive model with the implicit finite element method. Computational Materials Science, 2022, 208, 111348.	1.4	13
147	Effect of powder reuse on tensile, compressive, and creep strength of Inconel 718 fabricated via laser powder bed fusion. Materials Characterization, 2022, 190, 112023.	1.9	12
148	Processing of Dilute Mg–Zn–Mn–Ca Alloy/Nb Multilayers by Accumulative Roll Bonding. Advanced Engineering Materials, 2020, 22, 1900673.	1.6	11
149	Experimental verification of a crystal plasticity-based simulation framework for predicting microstructure and geometric shape changes: Application to bending and Taylor impact testing of Zr. International Journal of Impact Engineering, 2020, 144, 103655.	2.4	11
150	Crystal mechanics-based thermo-elastic constitutive modeling of orthorhombic uranium using generalized spherical harmonics and first-order bounding theories. Journal of Nuclear Materials, 2022, 560, 153472.	1.3	11
151	A new approach to fluid–structure interaction within graphics hardware accelerated smooth particle hydrodynamics considering heterogeneous particle size distribution. Computational Particle Mechanics, 2018, 5, 387-409.	1.5	10
152	Structure and properties of pseudomorphically transformed bcc Mg in Mg/Nb multilayered nanolaminates studied using synchrotron X-ray diffraction. Journal of Applied Physics, 2019, 126, 025302.	1.1	10
153	Role of microstructural heterogeneities in damage formation and fracture of oligocrystalline Mg under tensile loading. Materials Science & Engineering A: Structural Materials: Properties, Microstructure and Processing, 2021, 827, 142096.	2.6	10
154	Dislocation-induced plastic instability in a rare earth containing magnesium alloy. Materialia, 2021, 15, 101038.	1.3	9
155	Fatigue strength of additive manufactured Mar-M-509 superalloy. Materials Science & Engineering A: Structural Materials: Properties, Microstructure and Processing, 2022, 840, 142913.	2.6	9
156	Effect of Grain Shape on Texture Formation during Severe Plastic Deformation of Pure Copper. Advanced Engineering Materials, 2018, 20, 1600829.	1.6	8
157	Predicting extreme anisotropy and shape variations in impact testing of tantalum single crystals. International Journal of Solids and Structures, 2022, 241, 111466.	1.3	8
158	Material modeling and simulation of continuous-bending-under-tension of AA6022-T4. Journal of Materials Processing Technology, 2021, 287, 116658.	3.1	7
159	Dilational Response of Voided Polycrystals. Jom, 2017, 69, 942-947.	0.9	6
160	Microstructure Correlation with Formability for Biaxial Stretching of Magnesium Alloy AZ31B at Mildly Elevated Temperatures. Jom, 2017, 69, 907-914.	0.9	6
161	An automated procedure built on MTEX for reconstructing deformation twin hierarchies from electron backscattered diffraction datasets of heavily twinned microstructures. Materials Characterization, 2021, 171, 110808.	1.9	6
162	Viscoplastic self-consistent formulation as generalized material model for solid mechanics applications. Applications in Engineering Science, 2021, 6, 100040.	0.5	6

#	Article	IF	CITATIONS
163	Multi-strain path deformation behavior of AA6016-T4: Experiments and crystal plasticity modeling. International Journal of Solids and Structures, 2022, 244-245, 111536.	1.3	6
164	Coupling kinetic Monte Carlo and finite element methods to model the strain path sensitivity of the isothermal stress-assisted martensite nucleation in TRIP-assisted steels. Mechanics of Materials, 2021, 154, 103707.	1.7	5
165	Towards Manufacturing of Ultrafine-Laminated Structures in Metallic Tubes by Accumulative Extrusion Bonding. Metals, 2021, 11, 389.	1.0	5
166	Micromechanical origins of remarkable elongation-to-fracture in AHSS TRIP steels via continuous bending under tension. Materials Science & Engineering A: Structural Materials: Properties, Microstructure and Processing, 2021, 825, 141876.	2.6	5
167	Physical simulations of heat-affected zone microstructures to compare weldability characteristics of additively manufactured and wrought 17-4 stainless steel. Materials Characterization, 2022, 185, 111714.	1.9	5
168	Modeling cyclic plasticity of additively manufactured alloy Mar-M-509 using a high-performance spectral-based micromechanical model. Applications in Engineering Science, 2021, 7, 100065.	0.5	4
169	Efficient rolling texture predictions and texture-sensitive thermomechanical properties of α-uranium foils. Journal of Nuclear Materials, 2017, 495, 234-243.	1.3	3
170	Deformation-induced surface roughening of an Al-Mg alloy. Journal of Physics: Conference Series, 2018, 1063, 012132.	0.3	3
171	Mesoscale, Microstructure-Sensitive Modeling for Interface-Dominated, Nanostructured Materials. , 2018, , 1-42.		3
172	A shape interpolation procedure: Application to creating explicit grain structure models based on partial data sets. Computational Materials Science, 2019, 167, 42-51.	1.4	3
173	Adjustment of the Mechanical Properties of Mg2Nd and Mg2Yb by Optimizing Their Microstructures. Metals, 2021, 11, 377.	1.0	3
174	Modeling Tensile, Compressive, and Cyclic Response of Inconel 718 Using a Crystal Plasticity Model Incorporating the Effects of Precipitates. Minerals, Metals and Materials Series, 2018, , 655-668.	0.3	3
175	Inducing <111> texture in AA5182-O through continuous-bending-under-tension and recovery heat treatment processes to influence r-values. CIRP Annals - Manufacturing Technology, 2022, , .	1.7	3
176	Towards Computationally Tractable Simulations of Metal Forming Processes With Evolving Microstructures. , 2014, , .		1
177	Effect of Hot Working on the High Cycle Fatigue Behavior of WE43 Rare Earth Magnesium Alloy. Minerals, Metals and Materials Series, 2019, , 219-225.	0.3	1
178	Mesoscale, Microstructure-Sensitive Modeling for Interface-Dominated, Nanostructured Materials. , 2020, , 1111-1152.		1
179	Formability of Magnesium Alloy AZ31B from Room Temperature to 125°C Under Biaxial Tension. Minerals, Metals and Materials Series, 2017, , 661-667.	0.3	0
180	Formability Improvements of DP 1180 Subjected to Continuous-Bending-Under-Tension. IOP Conference Series: Materials Science and Engineering, 2018, 418, 012043.	0.3	0